Cementor

A toolbox to generate bio-cemented soils with specific microstructures

Zhang, Aoxi; Dieudonné, Anne Catherine

DOI
[10.1016/j.bgtech.2024.100081](https://doi.org/10.1016/j.bgtech.2024.100081)

Publication date
2024

Document Version
Final published version

Published in
Biogeotechnics

Important note
To cite this publication, please use the final published version (if applicable).
Please check the document version above.

Cementor: A toolbox to generate bio-cemented soils with specific microstructures

Aoxi Zhang[a], Anne-Catherine Dieudonné[a,*]

[a] *Geo-Engineering section, Faculty of Civil Engineering and Geosciences, Delft University of Technology, the Netherlands*

A B S T R A C T

Bio-cemented soils can exhibit various types of microstructure depending on the relative position of the carbonate crystals with respect to the host granular skeleton. Different microstructures can have different effects on the mechanical and hydraulic responses of the material, hence it is important to develop the capacity to model these microstructures. The discrete element method (DEM) is a powerful numerical method for studying the mechanical behaviour of granular materials considering grain-scale features. This paper presents a toolbox that can be used to generate 3D DEM samples of bio-cemented soils with specific microstructures. It provides the flexibility of modelling bio-cemented soils with precipitates in the form of contact cementing, grain bridging and coating, and combinations of these distribution patterns. The algorithm is described in detail in this paper, and the impact of the precipitated carbonates on the soil microstructure is evaluated. The results indicate that carbonates precipitated in different distribution patterns affect the soil microstructure differently, suggesting the importance of modelling the microstructure of bio-cemented soils.

1. Introduction

Inspired by natural processes, many innovative technologies have been developed as ecological alternatives in geotechnical engineering (DeJong et al., 2010; He et al., 2019; Martinez et al., 2022; Tang & Tao, 2022; Zhang et al., 2023). Microbially induced calcite precipitation (MICP), which has attracted attention in recent years, is one of them. MICP can be used for a wide range of applications spanning ground improvement (Fu et al., 2023; van Paassen et al., 2010; Xiao et al., 2022b; Zeng et al., 2021; Cheng et al., 2019, among others), liquefaction mitigation (Darby et al., 2019; Xiao et al., 2018, protection against soil erosion (ClaràSaracho et al., 2021; Jiang & Soga, 2017; Salifu et al., 2016; Shahin et al., 2020; Wang et al., 2023, dust control (Hamdan & Kavazanjian, 2016, heavy metal removal (Chen et al., 2017; Li et al., 2013,Li et al., 2016; Zeng et al., 2023, and remediation of desiccation cracking (Liu et al., 2020).

MICP involves biogeochemical processes to drive the precipitation of calcium carbonate, thereby cementing the soil and enhancing its mechanical properties. The enhancement of mechanical properties of MICP-treated soils is strongly related to their microstructure. Benefitting from techniques such as scanning electron microscope (SEM) (Cheng et al., 2016; Ma et al., 2022; Mujah et al., 2019,

computed tomography (CT) (Dadda et al., 2017; Terzis & Laloui, 2018) and microfluidic chip tests (Elmaloglou et al., 2022; Wang et al., 2019; Xiao et al., 2021a,2022a), crystal size, shape, growth pattern and distribution pattern of the precipitated calcium carbonate can be assessed. In particular, soils treated by MICP were found to exhibit typical microstructures depending on the location of the precipitated carbonate particles with respect to the host granular skeleton (Fig. 1). In general, three basic distribution patterns of calcium carbonate can be observed experimentally (Kajiyama et al., 2017; Van Paassen, 2009; Xiao et al., 2021b), as conceptualised and illustrated in Fig. 1: (1) particle bridging, where carbonate crystals fill the gap between two host grains which are initially not in contact with each other, (2) contact cementing, where $CaCO_3$ particles are located at the contact between two host grains, and (3) particle coating, where the crystals are attached to the surface of host grains. The distribution pattern of the precipitated carbonates is found to be affected and partly controlled by factors such as soil saturation degree (Cheng et al., 2013, urease activity (Cheng et al., 2019 and the solution pH (Okwadha & Li, 2010).

Being able to model explicitly the different microstructures of bio-cemented soils is an important step towards a better understanding of the material behaviour and thus facilitating the applications of MICP. The discrete element method (DEM) has been extensively used to

---
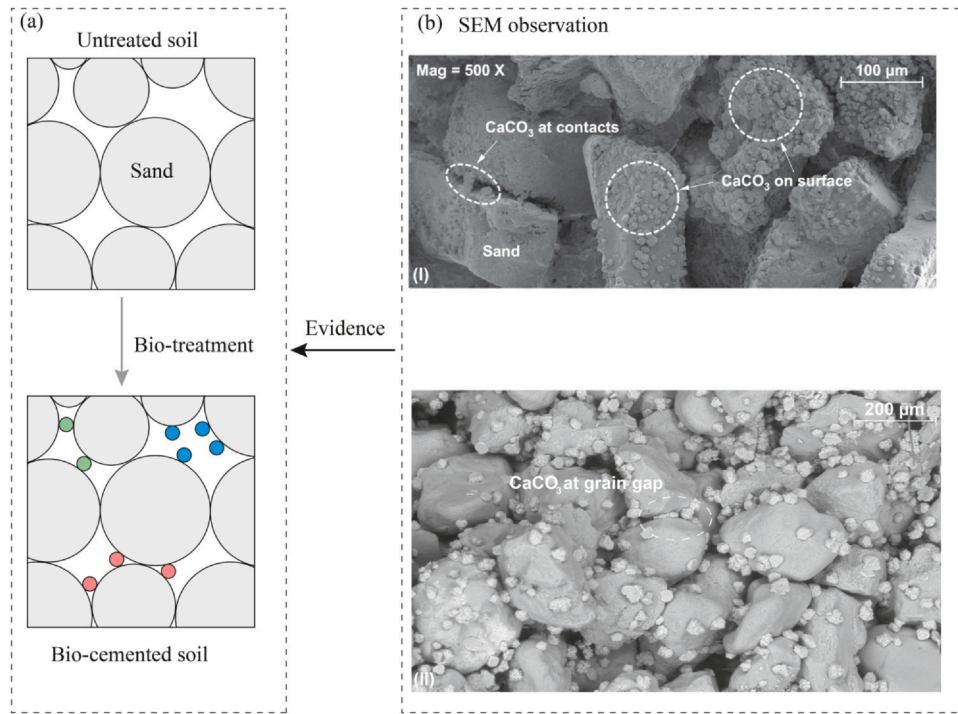
Fig. 1. Conceptual representation of the microstructure of bio-cemented soils: (a) 2D schematics, and (b) experimental observations. SEM picture (i) is cited from Xiao et al. (2021b) and SEM picture (ii) is from Van Paassen (2009). CaCO₃ in different distribution patterns are characterised by different colours.

investigate the behaviour of cemented granular materials. A common approach to modeling these materials is to introduce virtual bonds (such as parallel bonds) between host grains to mimic the function of carbonate particles (referred to as fines in the present paper) (Feng et al., 2017; Shen et al., 2016; Utili & Nova, 2008; Yang et al., 2019. However, this approach is not able to capture the effect of various microstructures as the virtual bonds can only be deployed at existing grain contacts. Explicitly modelling the cohesive particles in host sands can address this problem (Wang & Leung, 2008; Wu et al., 2023; Zhang & Dieudonné, 2023a,b). In this paper, we present a toolbox that can be used to model 3D cemented granular assemblies with diverse microstructures. The toolbox, named Cementor, is based on the open-source DEM platform YADE. The algorithms of the toolbox are first described in detail. Microscopic observations on the 3D DEM bio-cemented samples are then presented.

2. 3D DEM modelling of various microstructures of bio-cemented soil

The toolbox aims to introduce fine spherical particles at specific positions within an assembly made up of spherical grains. The toolkit enables the modelling of various types of microstructures, including bridging, contact cementing, coating, and combinations thereof. Cementor is compatible with the open-source platform for discrete element modelling YADE (Yet another dynamic engine) (Šmilauer et al., 2021).

The overall structure and the algorithms for modelling the different distribution patterns are described in the following sections. The term "fine" is used to refer to the carbonate particles in soils treated by MICP.

2.1. Overall structure

The flowchart to generate cemented samples with a single distribution pattern is presented in Fig. 2. The procedure starts with importing a host sample (the generation of the host sample is not covered in this study but can be found in YADE examples). Thereafter, all particles need to be fixed by blocking all their degrees of freedom, which
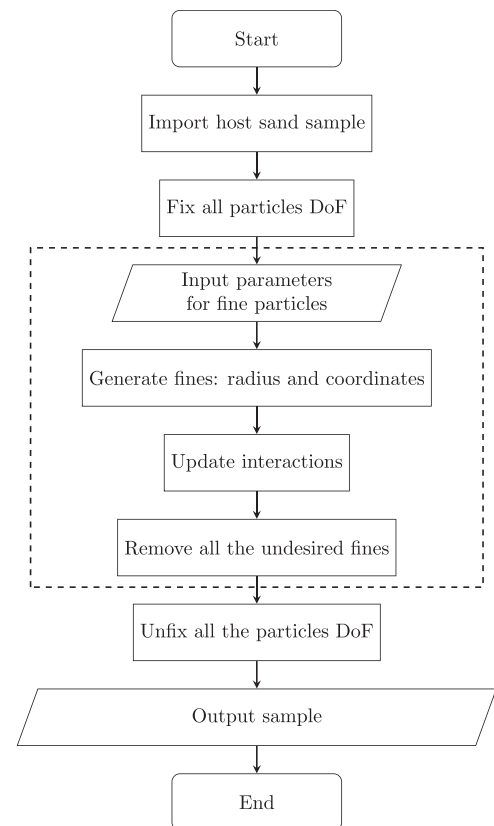
Fig. 2. Flowchart for generating samples containing fines with various microstructures.

ensures that the initial fabric of the host material is preserved during the process of introducing fines. The fines generation process, indicated inside the dashed rectangle zone in Fig. 2, starts after that. It contains four steps:

Table 1
Input parameters for controlling the number and size of fines.

Microstructure type	Input parameters
Bridging	TR_{min}, TR_{max}
Contact cementing	T_{CC}, N_{CC}
Coating	T_{CO}, N_{CO}, α

1. **Enter input parameters**. Different input parameters are used to generate the target microstructure, as summarised in Table 1. The input parameters control the number and size of the fines to be generated and, therefore, the fine content of the sample. The fine content can be defined by the user. For example, the fine mass content is the ratio of the mass of fines to the mass of the host material. The meaning of each parameter is given in the following subsections. Besides the input parameters listed in Table 1, other parameters such as those related to the material properties (density, Young's modulus, etc.) and contact properties (friction angle, cohesive strength, etc.) need to be introduced. These are not discussed in this paper as they depend on the specific material and contact laws selected by the user.
2. **Generate raw fines with a defined distribution pattern**. At this stage, the radius and coordinates of the fines are computed using the algorithms described in the following subsections.
3. **Update interactions**. The newly generated fines have not been assigned with interactions. Therefore, we run a "blank" step to detect contact and build interactions.
4. **Remove the undesired fines from the raw fines**. Part of the raw fines generated in step 2 may be problematic. For instance, they can unreasonably penetrate into other particles. These fines are undesired, and they are removed at this stage. Note that the criterion for removing undesired fines varies depending on the target microstructure. According to the definition of each type of microstructure, a fine particle in the pattern of bridging has two sand-fine contacts, a fine particle in the pattern of contact cementing has two sand-fine contacts and two fine-fine contacts, and a fine particle in the coating pattern has one sand-fine contact. Therefore, the fines whose number of interactions is not equal to 2 in the case of bridging, 4 in the case of contact cementing, and 1 in the case of coating will be removed.

After the above-described steps, the fixed particles are set free by unblocking all their degrees of freedom. Finally, the cemented sample can be saved.

The algorithms used to generate raw fines, as mentioned in step 2, are described in the following subsections.

2.2. Single distribution pattern

2.2.1. Bridging

Bridging refers to the distribution of fines which fill in the gaps between sand grains. The gap size distribution is a known feature for a given host sand sample. Therefore, we reproduce the bridging type of microstructure by defining the target minimum and maximum radii of fines, TR_{min} and TR_{max}. In the code, we loop through all pairs of sand particles to get the coordinates of the centres of both sand particles, C_{s1} and C_{s2}, and their radii r_{s1} and r_{s2}. The gap distance d of this pair of sand particles is calculated as:

$$d = ||\overrightarrow{C_{s1}C_{s2}}|| - r_{s1} - r_{s2} \tag{1}$$

as depicted in Fig. 3. For gaps that satisfy $TR_{min} \leq d \leq TR_{max}$, a fine particle of radius $r = d/2$ is inserted. It should be noted that r is a theoretical value while the computation is done with a finite precision. Therefore, it is suggested to slightly round up r to facilitate contact detection in DEM. The centre C_f of the fine particle to be introduced is
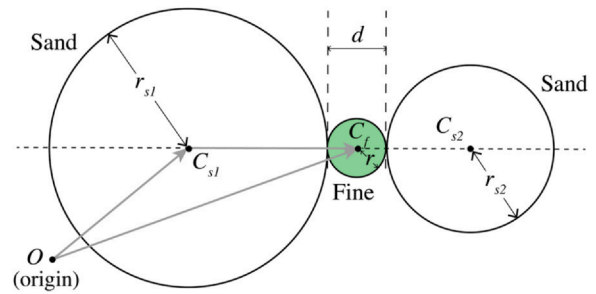

Fig. 3. Illustration of calculation for bridging pattern.

given by its position vector:

$$\overrightarrow{OC_f} = \overrightarrow{OC_{s1}} + \overrightarrow{C_{s1}C_f} = \overrightarrow{OC_{s1}} + (r_{s1} + r) \cdot \frac{\overrightarrow{C_{s1}C_{s2}}}{||\overrightarrow{C_{s1}C_{s2}}||} \tag{2}$$

where $O(0, 0, 0)$ is the origin of the space.

2.2.2. Contact cementing

Contact cementing refers to a microstructure where fines are located around the sand-sand contact points. Microscopic observations (Lin et al., 2016; Xiao et al., 2021b, 2022c, among others) have shown that carbonate particles located at sand-sand contacts can either form a complete ring or be located eccentrically on one side of the contact. The algorithm presented in this paper assumes a complete and intact ring. Other cases can be easily tackled by removing some particles from the intact ring.

For a given host sand sample, the existing sand-sand contacts can be accessed from YADE. A percentage T_{CC} of all sand-sand contacts is randomly selected in order to be cemented. For each selected sand-sand contact, a set of fines are introduced around the sand-sand contact point, forming a chain (Fig. 4). All fines of a given chain are in contact with each other and have the same size. The number of fines in each chain N_{CC} is an input parameter. The radius r of the fines can then be determined from the input parameter N_{CC}, the radii of the two sand particles in contact, r_{s1} and r_{s2}, and the overlap d of these two sand grains. These last quantities can be obtained from YADE.

The fine radius r can be expressed as (Fig. 4):

$$r = r_c \sin\left(\frac{\pi}{N_{CC}}\right) \tag{3}$$

where the chain radius r_c is given by (Fig. 4):

$$r_c = \sqrt{(r_{s1} + r)^2 - \left(r_{s1} - \frac{d}{2} + h\right)^2} \tag{4}$$

with h, the distance between the contact point P and the chain centre C_c, given by:
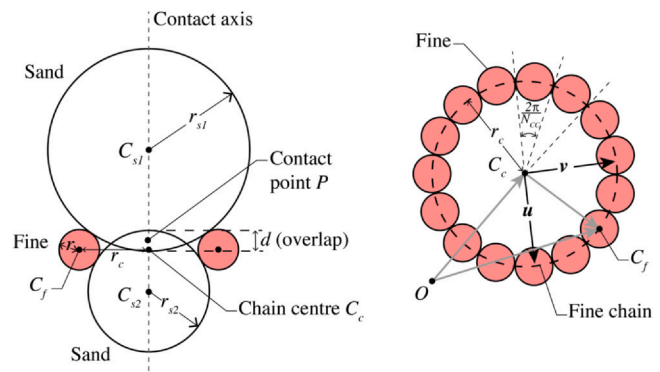

Fig. 4. Illustration of calculation for contact cementing pattern, demonstrated with 15 fines on a chain.

$$h = \frac{(r_{s1} - r_{s2})\left(r + \frac{d}{2}\right)}{r_{s1} + r_{s2} - d} \tag{5}$$

Note that the contact point P lies along the line connecting C_{s1} and C_{s2}, and is the middle point of the overlap.

The coordinates of all N_{CC} fines of a given chain can be determined by knowing the position of any of these fines. Therefore, the coordinates of the chain centre C_c should first be obtained. Its position vector is given by:

$$\vec{OC_c} = \vec{OP} + h \cdot \vec{j} \tag{6}$$

where the coordinates of the contact point P are known from YADE, and $\vec{j}$ is a unit vector whose direction is from the centre of the sand particle with the largest radius towards the centre of the sand particle with the smallest radius. Accordingly, it is defined as:

$$\vec{j} = \frac{\vec{C_{s1}C_{s2}}}{\|\vec{C_{s1}C_{s2}}\|} \tag{7}$$

where C_{s1} and C_{s2} are known from YADE.

After C_c is obtained, the coordinates of the fine particles in the chain are calculated as follows:

1. Define a non-zero vector $\vec{w}$ orthogonal to $\vec{j} = (a, b, c)$. In 3D, there is an infinite number of vectors perpendicular to $\vec{j}$. We construct one of them, $\vec{w}$, according to the following strategy. We initially set $\vec{w} = (a, b, c)$, and then find out the smallest coordinate a, b or c in absolute value. We set this value to zero, and swap the other two coordinates and negate the first one. For example, if $|a| \le |b|$ and $|a| \le |c|$, set a to 0, swap b and c and negate c. Consequently, $\vec{w} = (0, -c, b)$. Thereby, $\vec{w}$ is perpendicular to $\vec{j}$ at any time, since $\vec{j} \cdot \vec{w} = a0 - bc + cb = 0$.

2. Convert $\vec{w}$ into a vector $\vec{u}$ of magnitude r_c:

$$\vec{u} = r_c \frac{\vec{w}}{\|w\|} \tag{8}$$

3. Construct a vector $\vec{v}$ perpendicular to $\vec{j}$ and $\vec{u}$ such that:

$$\vec{v} = \vec{j} \times \vec{u} \tag{9}$$

4. Determine the coordinates of the centre C_f of one of the fines as:

$$\vec{OC_f} = \vec{OC_c} + \vec{C_cC_f} = \vec{OC_c} + \vec{u}\cos(\alpha) + \vec{v}\sin(\alpha) \tag{10}$$

where α is an arbitrary angle.

5. Compute all N_{CC} coordinates of the fines centres on the chain as:

$$\vec{OC_f^k} = \vec{OC_c} + \vec{u}\cos\left(\frac{2\pi k}{N_{CC}}\right) + \vec{v}\sin\left(\frac{2\pi k}{N_{CC}}\right). \tag{11}$$

where $k = 0, 1, 2, \ldots, N_{CC} - 1$.

The above algorithm is applied on all the selected sand-sand contacts, so that all raw fines with contact cementing type of microstructure are obtained.
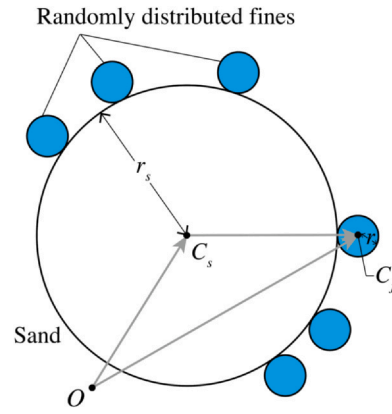

Fig. 5. Illustration of calculation for coating pattern.

2.2.3. Coating

Coating refers to a microstructure where fines attach to one sand grain only. There are three input parameters controlling the number and size of coating fines: the proportion of sand particles to be coated (T_{CO}), the target number of fines coating each selected sand grain (N_{CO}), and the ratio of the radius of the coated sand particle over the radius of fine particle (α). Accordingly, in the case of coating, the fine size is linked to the coated sand grain such that $r = \alpha r_s$. The sand particles to be coated are randomly selected from all the sand grains. For each of the selected sand grains, the fines are randomly distributed on the surface of that sand grain, as demonstrated in Fig. 5. The coordinates of the centre of each fine is given by:

$$\vec{OC_f} = \vec{OC_s} + (r_s + r)\vec{n} \tag{12}$$

where $\vec{n}$ is a random unit vector in the 3D space. Note that since the fines are randomly generated, it is possible that the generated fines overlap with each other, which may cause large repulsive force and an unstable situation. These fines can be detected since their number of interactions is larger than one, and they will be removed as described in Fig. 2.

2.3. Mixed-type microstructure

The toolbox is able to generate samples with mixed distribution patterns, namely, a sample exhibiting more than one microstructure pattern. Therefore, the functions for generating the involved microstructures can be activated by assigning the input parameters as listed in Table 1 to the corresponding functions. The process is the same as described in Fig. 2. Specifically, fines with each type of microstructure are generated separately. After that, all the generated fines are assessed to identify the undesired fines. The criterion for determining the undesired fines is the same as described before. Finally, all the undesired fines are removed, and the sample with fines is output.

3. Microscopic observations

In a MICP treatment, carbonate crystals can precipitate in different distribution patterns in the soils, which may lead to different changes in the soil microstructure. In this section, $CaCO_3$ precipitation-induced microstructure change is evaluated in terms of effective coordination number and contact distribution. To achieve this goal, a 3D DEM

uncemented sample is first generated (more details can be found in Zhang and Dieudonné (2023b)). After that, carbonate particles with different contents (defined as the mass of CaCO$_3$ divided by the mass of the sample) and distribution patterns (i.e. bridging, contact cementing and coating) are introduced into the uncemented sample. In this way, the original fabric of the sand particles is the same in all the cemented samples. Accordingly, the effect of each carbonate distribution pattern on the soil microstructure can be assessed individually. The information of the bio-cemented samples illustrated here is summarized in Table 2.

3.1. Effective coordination number

The coordination number and the mechanical coordination number are commonly used indexes to describe the state of a granular packing (Dai, Yang, & Luo, 2015; Gu, Zhang, & Huang, 2020; Thornton, 2000; Yang, Kavazanjian, & Neithalath, 2019. However, there are limitations in using these two indexes to describe a bio-cemented sample when the carbonate particles are explicitly modelled (Zhang & Dieudonné, 2023b). Therefore, this section evaluates the change in the effective coordination number due to the carbonate precipitation.

The effective coordination number Z_e describes the average number of effective bonds per sand grain. It is defined as:

$$Z_e = \frac{2(C_s + C_b)}{N_s} \qquad (13)$$

where N_s is the number of sand particles in the sample, C_s is the total number of sand-sand contacts and C_b is the number of effective bond in the sample. In the case of a bridging type of cementation, each carbonate initially connects two sand grains that forms an effective bond. Therefore, C_b is equal to the number of carbonate particles at the initial state. In terms of contact cementing type cementation, several carbonates form a cement chain and, together, strengthen one sand-sand contact. Therefore, in this case, C_b is equal to the number of intact cement chains. Note that the cemented contacts are counted twice in the proposed definition of the effective coordination number. This is meant to reflect the fact that, in the case of contact cementing, two components contribute together to the mechanical response of the contact: the sand-sand contact, which is purely frictional, and the part from the cohesive carbonates. In the case of coating, C_b is equal to zero as carbonate particles do not introduce connections between sand grains.

Fig. 6 shows the evolution of the effective coordination number with respect to carbonate content. It can be seen that the introduction of carbonates in the coating pattern does not lead to any change in Z_e compared to that of the uncemented sample. This is aligned with the physics that carbonates in the coating pattern do not form any effective connection between sand grains. By contrast, contact cementing and
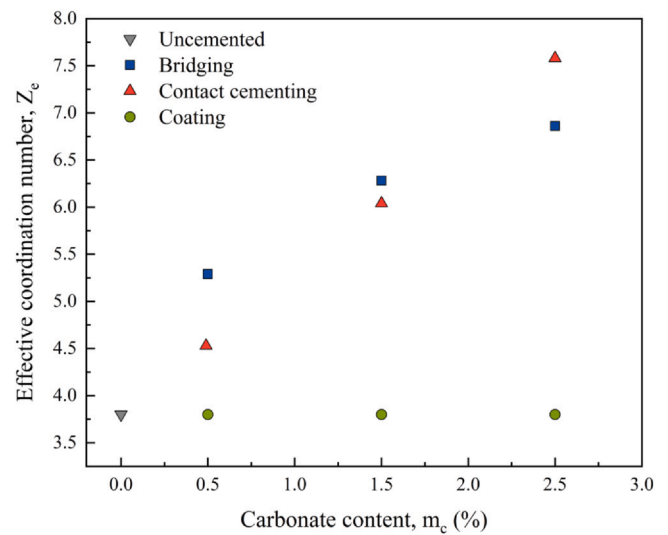

Fig. 6. Effective coordination number of uncemented sample and bio-cemented samples with different carbonate distribution patterns and contents.

bridging cases exhibit obvious increases in Z_e. The higher the carbonate content, the higher Z_e they show. In addition, given the same amount of carbonates, the bridging type of sample tends to present higher Z_e than that of the contact cementing type of sample at a lower carbonate content. As the carbonate content increases, the contact cementing case can exhibit a higher Z_e than the bridging case.

3.2. Contact normal distribution

The constitutive behaviour of soils is largely affected by their fabric, which is associated with the arrangement of soil grains. In this section, the change of soil fabric due to the introduction of CaCO$_3$ is investigated. The arrangement of particles is described by the contact orientation distribution in this study. The orientation of a contact between particles is described by the contact normal unit vector, which is the normal unit vector along the line connecting the centres of the two spheres in contact. It should be noted that, as there are sand and carbonate particles in a cemented sample, the contact normal distribution is demonstrated in terms of all inter-particle contacts, sand-carbonate (S-C) contacts and carbonate-carbonate (C-C) contacts.

Fig. 7 shows the orientation distribution of the contact unit normal vectors of DEM samples with different characteristics using a rose diagram in 3 planes, i.e. X-Y (left column), X-Z (middle column) and Z-Y plane (right column), respectively. In a rose diagram, each branch

Table 2
Information of the DEM samples.

Microstructure type	Input parameters	CaCO$_3$ number	Content (%)
Bridging	$TR_{min} = 0.0003$, $TR_{max} = 0.00054$	5185	0.5
	$TR_{min} = 0.0003$, $TR_{max} = 0.000703$	8674	1.5
	$TR_{min} = 0.0003$, $TR_{max} = 0.000803$	10675	2.5
Contact cementing	$T_{CC} = 19$, $N_{CC} = 15$	37905	0.49
	$T_{CC} = 59$, $N_{CC} = 15$	117630	1.5
	$T_{CC} = 99.5$, $N_{CC} = 15$	198210	2.5
Coating	$T_{CO} = 13$, $N_{CO} = 50$, $\alpha = 6.67$	10391	0.5
	$T_{CO} = 47$, $N_{CO} = 50$, $\alpha = 6.67$	32164	1.5
	$T_{CO} = 100$, $N_{CO} = 50$, $\alpha = 6.67$	55312	2.5

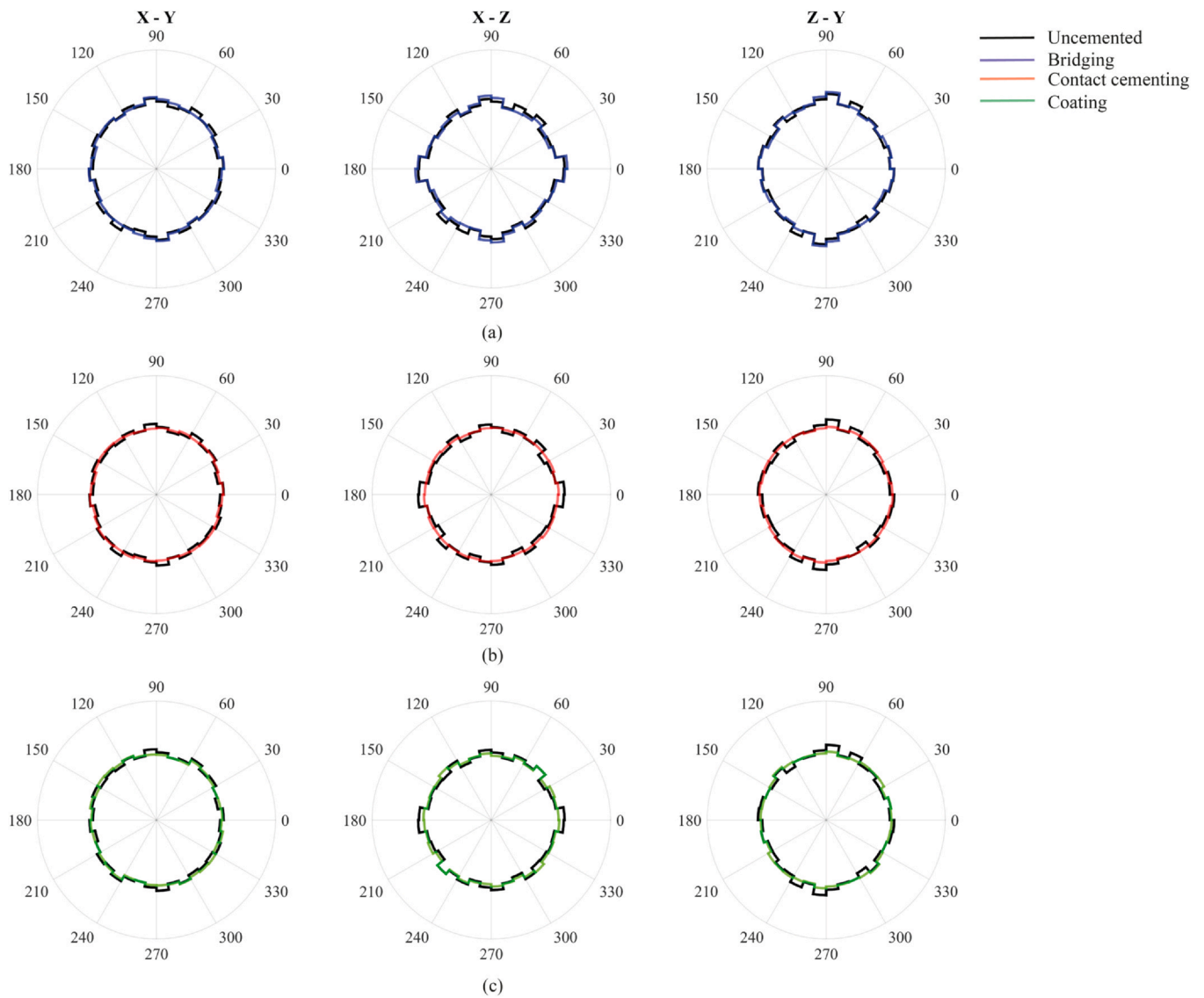Note: The unit of TR_{min} and TR_{max} is metre (m).

Fig. 7. Contact normal distribution of all inter-particle contacts: (a) bridging; (b) contact cementing; (c) Coating. The contact normal distribution of the uncemented sample is also plotted in each figure.

represents the normalised number of contact unit normal vectors that are located in the space interval. The cemented samples presented in Fig. 7 have the same carbonate content (1.5%). The contact normal distribution of the uncemented sample is also plotted so that the fabric changes caused by the introduction of CaCO$_3$ can be evaluated. It can be seen from Fig. 7(a) the contact orientation distribution of bridging is almost the same as that of the uncemented sample, suggesting that CaCO$_3$ distributed in the pattern of bridging does not change the fabric much. As shown in Fig. 7(b) and (c), a more uniform contact orientation distribution can be found in the case of contact cementing and coating compared to the uncemented sample. As all the samples have the same sand-sand fabric, the difference in the orientation distribution of all

inter-particle contacts mainly comes from that of the sand-carbonate contacts. Fig. 8 compares the orientation distribution of sand-carbonate contacts between bridging, contact cementing and coating types of cemented samples with the same carbonate content (1.5%). It can be seen that contact cementing and coating cases present a more uniform distribution than bridging, consequently leading to a uniform distribution of all inter-particle contacts. It should be noted that there are also carbonate-carbonate contacts in contact cementing type of samples. The orientation distribution of carbonate-carbonate contacts in contact cementing type of cemented sample with 1.5% carbonate content is plotted in Fig. 9, which shows a uniform distribution in general.
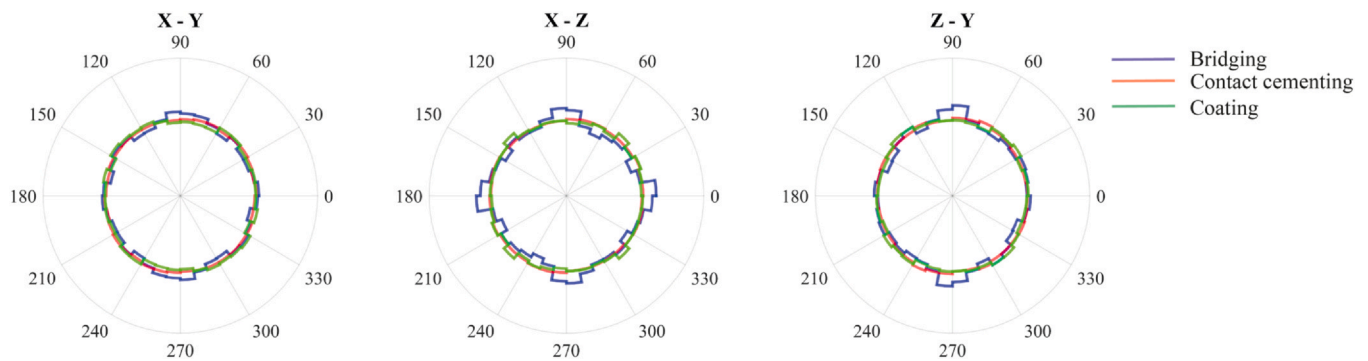
Fig. 8. Comparison of contact normal distribution of sand-carbonate contacts between bridging, contact cementing and coating type of cemented samples.
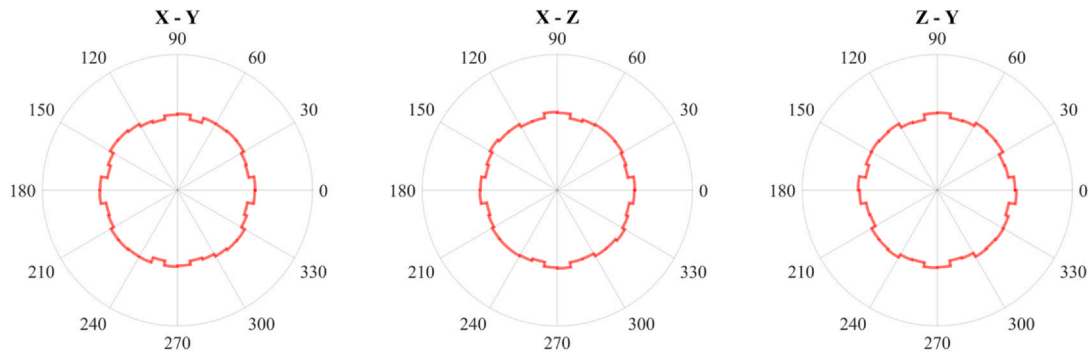

Fig. 9. Contact normal distribution of carbonate-carbonate contacts in contact cementing type of cemented sample.

4. Conclusions

Bio-cemented soils exhibit characteristic microstructures, which affect the mechanical and hydraulic behaviour of the materials. Being able to model explicitly the different microstructures is an important step towards a better understanding of the material behaviour from the microscopic point of view.

This paper presents a toolbox designed to introduce carbonate particles following different target microstructures within a granular packing. Three types of basic patterns are considered, namely bridging, contact cementing and coating. Modelling packings with mixed distribution patterns of carbonates is also possible using the provided algorithm. Using the developed toolbox, bio-cemented samples with different carbonate distribution patterns and contents are modelled, and the microscopic properties, such as the effective coordination number and contact orientation distribution, are investigated to reveal how the introduction of carbonates affects the soil microstructure. It is found that carbonates precipitated in different distribution patterns change differently in the effective coordination number. Specifically, carbonates in the coating pattern do not lead to a change in the effective coordination number, while carbonates in the bridging and contact cementing patterns present an obvious increase in the effective co-ordination number. In addition, the introduction of carbonates affects the soil fabric in terms of the contact normal distribution. Carbonates precipitated in the bridging pattern do not change the fabric much. By contrast, contact cementing and coating cases tend to form a more uniform contact normal distribution than that of the uncemented sample. In the future, improvements to the toolbox can be made by addressing its current limitations, including the integration of more realistic shapes for sand grains and precipitated crystals, thereby broadening its applicability.

CRediT authorship contribution statement

Aoxi Zhang: Writing – original draft, Visualization, Validation, Software, Methodology, Investigation, Formal analysis. **Anne-**

Catherine Dieudonné: Writing – review & editing, Supervision, Resources, Methodology, Conceptualization.

Declaration of Competing Interest

The authors declare the following financial interests/personal relationships which may be considered as potential competing interests: Aoxi Zhang reports financial support was provided by China Scholarship Council. If there are other authors, they declare that they have no known competing financial interests or personal relationships that could have appeared to influence the work reported in this paper.

References

Chen, X., Guo, H., & Cheng, X. (2017). Heavy metal immobilisation and particle cementation of tailings by biomineralisation. *Environmental Geotechnics, 5*, 107–113. https://doi.org/10.1680/jenge.15.00068

Cheng, L., Cord-Ruwisch, R., & Shahin, M. A. (2013). Cementation of sand soil by microbially induced calcite precipitation at various degrees of saturation. *Canadian Geotechnical Journal, 50*, 81–90. https://doi.org/10.1139/cgj-2012-0023

Cheng, L., Shahin, M. A., & Chu, J. (2019). Soil bio-cementation using a new one-phase low-pH injection method. *Acta Geotechnica, 14*, 615–626. https://doi.org/10.1007/s11440-018-0738-2

Cheng, L., Shahin, M. A., & Mujah, D. (2016). Influence of key environmental conditions on microbially induced cementation for soil stabilization. *Journal of Geotechnical and Geoenvironmental Engineering, 143*, Article 04016083. https://doi.org/10.1061/(ASCE)GT.1943-5606.00015

ClaràSaracho, A., Haigh, S. K., & EhsanJorat, M. (2021). Flume study on the effects of microbial induced calcium carbonate precipitation (MICP) on the erosional behaviour of fine sand. *Géotechnique, 71*, 1135–1149. https://doi.org/10.1680/jgeot.19.P.350

Dadda, A., Geindreau, C., Emeriault, F., DuRoscoat, S. R., Garandet, A., Sapin, L., & Filet, A. E. (2017). Characterization of microstructural and physical properties changes in biocemented sand using 3D X-ray microtomography. *Acta Geotechnica, 12*, 955–970. https://doi.org/10.1007/s11440-017-0578-5

Dai, B., Yang, J., & Luo, X. (2015). A numerical analysis of the shear behavior of granular soil with fines. *Particuology, 21*, 160–172. https://doi.org/10.1016/j.partic.2014.08.010

Darby, K. M., Hernandez, G. L., DeJong, J. T., Boulanger, R. W., Gomez, M. G., & Wilson, D. W. (2019). Centrifuge model testing of liquefaction mitigation via microbially induced calcite precipitation. *Journal of Geotechnical and Geoenvironmental Engineering, 145*, 04019084. https://doi.org/10.1061/(ASCE)GT.1943-5606.0002122

DeJong, J. T., Mortensen, B. M., Martinez, B. C., & Nelson, D. C. (2010). Bio-mediated soil improvement. *Ecological Engineering, 36*, 197–210. https://doi.org/10.1016/j.ecoleng.2008.12.029

Elmaloglou, A., Terzis, D., De Anna, P., & Laloui, L. (2022). Microfluidic study in a meter-long reactive path reveals how the medium's structural heterogeneity shapes MICP-induced biocementation. *Scientific Reports, 12*, 19553.

Feng, K., Montoya, B., & Evans, T. (2017). Discrete element method simulations of bio-cemented sands. *Computers and Geotechnics, 85*, 139–150. https://doi.org/10.1016/j.compgeo.2016.12.028

Fu, T., Saracho, A. C., & Haigh, S. K. (2023). Microbially induced carbonate precipitation (MICP) for soil strengthening: a comprehensive review. *Biogeotechnics, 100002*. https://doi.org/10.1016/j.bgtech.2023.100002

Gu, X., Zhang, J., & Huang, X. (2020). DEM analysis of monotonic and cyclic behaviors of sand based on critical state soil mechanics framework. *Computers and Geotechnics, 128*, 103787. https://doi.org/10.1016/j.compgeo.2020.103787

Hamdan, N., & Kavazanjian, E., Jr. (2016). Enzyme-induced carbonate mineral precipitation for fugitive dust control. *Géotechnique, 66*, 546–555. https://doi.org/10.1680/jgeot.15.P.168

He, J., Chu, J., Gao, Y., & Liu, H. (2019). Research advances and challenges in biogeo-technologies. *Geotechnical Research, 6*, 144–155. https://doi.org/10.1680/jgere.18.00035

Jiang, N. J., & Soga, K. (2017). The applicability of microbially induced calcite precipitation (MICP) for internal erosion control in gravel-sand mixtures. *Géotechnique, 67*, 42–55. https://doi.org/10.1680/jgeot.15.P.182

Kajiyama, S., Wu, Y., Hyodo, M., Nakata, Y., Nakashima, K., & Yoshimoto, N. (2017). Experimental investigation on the mechanical properties of methane hydrate-bearing sand formed with rounded particles. *Journal of Natural Gas Science and Engineering, 45*, 96–107. https://doi.org/10.1016/j.jngse.2017.05.008

Li, M., Cheng, X., & Guo, H. (2013). Heavy metal removal by biomineralization of urease producing bacteria isolated from soil. *International Biodeterioration & Biodegradation, 76*, 81–85. https://doi.org/10.1016/j.ibiod.2012.06.016

Li, M., Cheng, X., Guo, H., & Yang, Z. (2016). Biomineralization of carbonate by terra-bacter tumescens for heavy metal removal and biogrouting applications. *Journal of Environmental Engineering, 142*, C4015005. https://doi.org/10.1061/(ASCE)EE.1943-7870.0000970

Lin, H., Suleiman, M. T., Brown, D. G., & Kavazanjian, E., Jr. (2016). Mechanical behavior of sands treated by microbially induced carbonate precipitation. *Journal of Geotechnical and Geoenvironmental Engineering, 142*, 04015066. https://doi.org/10.1061/(ASCE)GT.1943-5606.0001383

Liu, B., Zhu, C., Tang, C. S., Xie, Y. H., Yin, L. Y., Cheng, Q., & Shi, B. (2020). Bio-remediation of desiccation cracking in clayey soils through microbially induced calcite precipitation (MICP). *Engineering Geology, 264*, 105389. https://doi.org/10.1016/j.enggeo.2019.105389

Ma, G., Xiao, Y., Fan, W., Chu, J., & Liu, H. (2022). Mechanical properties of biocement formed by microbially induced carbonate precipitation. *Acta Geotechnica, 1–15*.

Martinez, A., DeJong, J., Akin, I., Aleali, A., Arson, C., Atkinson, J., ... Boulanger, R., et al. (2022). Bio-inspired geotechnical engineering: Principles, current work, opportunities and challenges. *Géotechnique, 72*, 687–705. https://doi.org/10.1680/jgeot.20.P.170

Mujah, D., Cheng, L., & Shahin, M. A. (2019). Microstructural and geomechanical study on biocemented sand for optimization of MICP process. *Journal of Materials in Civil Engineering, 31*, Article 04019025.

Okwadha, G. D., & Li, J. (2010). Optimum conditions for microbial carbonate precipitation. *Chemosphere, 81*, 1143–1148.

Salifu, E., MacLachlan, E., Iyer, K. R., Knapp, C. W., & Tarantino, A. (2016). Application of microbially induced calcite precipitation in erosion mitigation and stabilisation of sandy soil foreshore slopes: A preliminary investigation. *Engineering Geology, 201*, 96–105. https://doi.org/10.1016/j.enggeo.2015.12.027

Shahin, M., Jamieson, K., & Cheng, L. (2020). Microbial-induced carbonate precipitation for coastal erosion mitigation of sandy slopes. *Géotechnique Letters, 10*, 211–215. https://doi.org/10.1680/jgele.19.00093

Shen, Z., Jiang, M., & Thornton, C. (2016). DEM simulation of bonded granular material. part I: contact model and application to cemented sand. *Computers and Geotechnics, 75*, 192–209.

Šmilauer, V., et al. (2021). *Yade Documentation* (3rd ed..,). The Yade Project,. 10.5281/zenodo.5705394 ⟨http://yade-dem.org/doc/⟩.

Tang, Y., & Tao, J. (2022). Multiscale analysis of rotational penetration in shallow dry sand and implications for self-burrowing robot design. *Acta Geotechnica, 17*, 4233–4252. https://doi.org/10.1007/s11440-022-01492-x

Terzis, D., & Laloui, L. (2018). 3-D micro-architecture and mechanical response of soil cemented via microbial-induced calcite precipitation. *Scientific Reports, 8*, 1416.

Thornton, C. (2000). Numerical simulations of deviatoric shear deformation of granular media. *Géotechnique, 50*, 43–53.

Utili, S., & Nova, R. (2008). DEM analysis of bonded granular geomaterials. *The International Journal for Numerical and Analytical Methods in Geomechanics, 32*, 1997–2031. https://doi.org/10.1002/nag.728

van Paassen, L. A., Ghose, R., van der Linden, T. J., van der Star, W. R., & van Loosdrecht, M. C. (2010). Quantifying biomediated ground improvement by ureolysis: large-scale biogrout experiment. *Journal of Geotechnical and Geoenvironmental Engineering, 136*, 1721–1728. https://doi.org/10.1061/(ASCE)GT.1943-5606.0000382

Van Paassen, L. A. (2009). *Biogrout, ground improvement by microbial induced carbonate precipitation. Ph.D. thesis.* Delft University of Technology.

Wang, Y. H., & Leung, S. C. (2008). A particulate-scale investigation of cemented sand behavior. *Canadian Geotechnical Journal, 45*, 29–44. https://doi.org/10.1139/T07-070

Wang, Y. N., Li, S. K., Li, Z. Y., & Garg, A. (2023). Exploring the application of the MICP technique for the suppression of erosion in granite residual soil in shantou using a rainfall erosion simulator. *Acta Geotechnica, 1–13*.

Wang, Y., Soga, K., DeJong, J. T., & Kabla, A. J. (2019). Microscale visualization of microbial-induced calcium carbonate precipitation processes. *Journal of Geotechnical and Geoenvironmental Engineering, 145*, 04019045. https://doi.org/10.1061/(ASCE)GT.1943-5606.0002079

Wu, H., Wu, W., Liang, W., Dai, F., Liu, H., & Xiao, Y. (2023). 3D DEM modeling of biocemented sand with fines as cementing agents. *International Journal for Numerical and Analytical Methods in Geomechanics, 47(2), 212–240*.

Xiao, Y., He, X., Stuedlein, A. W., Chu, J., Evans, T. M., & van Paassen, L. A. (2022a). Crystal growth of MICP through microfluidic chip tests. *Journal of Geotechnical and Geoenvironmental Engineering, 148*, Article 06022002. https://doi.org/10.1061/(ASCE)GT.1943-5606.0002756

Xiao, Y., He, X., Wu, W., Stuedlein, A. W., Evans, T. M., Chu, J., Liu, H., van Paassen, L. A., & Wu, H. (2021a). Kinetic biomineralization through microfluidic chip tests. *Acta Geotechnica, 16*, 3229–3237.

Xiao, Y., He, X., Zaman, M., Ma, G., & Zhao, C. (2022b). Review of strength improvements of biocemented soils. *International Journal of Geomechanics, 22*, Article 03122001.

Xiao, P., Liu, H., Xiao, Y., Stuedlein, A. W., & Evans, T. M. (2018). Liquefaction resistance of bio-cemented calcareous sand. *Soil Dynamics and Earthquake Engineering, 107*, 9–19. https://doi.org/10.1016/j.soildyn.2018.01.008

Xiao, Y., Stuedlein, A. W., He, X., Evans, T. M., Pan, Z., Lin, H., Chu, J., & Van Paassen, L. (2021b). Lateral responses of a model pile in biocemented sand. *International Journal of Geomechanics, 21*, Article 06021027.

Xiao, Y., Xiao, W., Wu, H., Liu, Y., & Liu, H. (2022c). Fracture of interparticle MICP bonds under compression. *International Journal of Geomechanics, 23*, Article 04022316.

Yang, P., Kavazanjian, E., & Neithalath, N. (2019). Particle-scale mechanisms in undrained triaxial compression of biocemented sands: insights from 3D DEM simulations with flexible boundary. *International Journal of Geomechanics, 19*, Article 04019009. https://doi.org/10.1061/(ASCE)GM.1943-5622.0001346

Zeng, Y., Chen, Z., Lyu, Q., Cheng, Y., Huan, C., Jiang, X., ... Tan, Z. (2023). Microbiologically induced calcite precipitation for in situ stabilization of heavy metals contributes to land application of sewage sludge. *Journal of Hazardous Materials, 441*, 129866. https://doi.org/10.1016/j.jhazmat.2022.129866

Zeng, C., Veenis, Y., Hall, C. A., Young, E. S., van Der Star, W. R., Zheng, J.j., & Van Paassen, L. A. (2021). Experimental and numerical analysis of a field trial application of microbially induced calcite precipitation for ground stabilization. *Journal of Geotechnical and Geoenvironmental Engineering, 147*, Article 05021003. https://doi.org/10.1061/(ASCE)GT.1943-5606.0002545

Zhang, A., & Dieudonné, A. C. (2023a). *Effects of carbonate distribution inhomogeneity on the improvement level of bio-cemented sands: A DEM study. International Conference of the International Association for Computer Methods and Advances in Geomechanics.* Springer554–561.

Zhang, A., & Dieudonné, A. C. (2023b). Effects of carbonate distribution pattern on the mechanical behaviour of bio-cemented sands: A DEM study. *Computer and Geotechnics, 154*, Article 105152.

Zhang, W., Xiang, J., Huang, R., & Liu, H. (2023). A review of bio-inspired geotechnics-perspectives from geomaterials, geo-components, and drilling & excavation strategies. *Biogeotechnics, 1*, 100025. https://doi.org/10.1016/j.bgtech.2023.100025